Electrostatic plasmon resonances of metal nanospheres in layered geometries

Jesper Jung,[1,*] Thomas Garm Pedersen,[1,2] Thomas Søndergaard,[1] Kjeld Pedersen,[1,2] Arne Nylandsted Larsen,[3,2] and Brian Bech Nielsen[3,2]

[1]*Department of Physics and Nanotechnology, Aalborg University, Skjernvej 4A, DK-9220 Aalborg Øst, Denmark*

[2]*Interdisciplinary Nanoscience Center (iNANO), Denmark*

[3]*Department of Physics and Astronomy, Aarhus University, DK-8000 Aarhus C, Denmark*

(Received 6 January 2010; revised manuscript received 10 February 2010; published 15 March 2010)

Electrostatic plasmon resonances of metal nanospheres situated in a stratified medium are analyzed theoretically utilizing a Green's function surface integral equation method. An efficient scheme for direct calculation of both particle plasmon eigenfrequencies and absorption cross sections is presented. By means of symmetry considerations we reduce the three-dimensional analysis to a single integral along the polar angle of the nanosphere and we show how all effects of the stratified surrounding can be built into the Green's function. We exemplify our approach by calculating the plasmon eigenfrequencies and absorption cross sections of silver nanospheres above a silicon surface and within a thin silicon film. The analysis of such configurations is important for plasmon enhanced solar cells.

DOI: 10.1103/PhysRevB.81.125413 PACS number(s): 41.20.Cv, 73.20.Mf, 02.30.Rz, 02.60.Cb

I. INTRODUCTION

It is well known that the strong colors of metallic nanoparticles are caused by collective excitations of the free conduction electrons of the particles. Such excitations are known as *particle plasmons* or *localized surface plasmons*, and have resonance frequencies that in general are dependent on the particle geometry, size, local dielectric surrounding, and the material that the particle is made from. One consequence of these localized surface plasmon resonances is that the near field around metallic nanoparticles can be orders of magnitude stronger than the incident field. Another is that the incident field gets strongly scattered for wavelengths close to the resonance. These properties suggest a variety of applications of metal nanoparticles. A few examples are plasmon enhanced solar cells[1–7] and different sensing applications[8] as, e.g., surface enhanced raman scattering[9] and biomedical detection.[10,11]

For a long time it has been known that light scattering from a spherical particle in a homogenous surrounding can be analyzed analytically.[12,13] The more complicated configuration, where a sphere is within close proximity of a surface has also been studied quite extensively, both for a single sphere, a dimer of spheres, and clusters of spheres.[14–20] However, in general for complex geometries and inhomogeneous surroundings where, e.g., one or more particles are close to a surface or embedded within a thin film, the analysis must often be performed utilizing advanced numerical techniques such as, e.g., finite difference time domain (FDTD),[21] finite element (FE),[22] or Green's function integral[23,24] approaches.

In this work, we are interested in analyzing geometries, which potentially are important for the development of plasmon enhanced solar cells; a small metallic nanoparticle embedded in a thin silicon film or placed near a silicon surface. The relevance for solar cells comes from the fact that scattering resonances can be tuned over a wide wavelength range via careful design of the surrounding geometry. In particular resonances in the infrared can be realized by embedding the nanoparticle in a layer of high refractive index material. The configuration, where the particle is embedded in a thin film, has not been much studied. In Ref. 25 the radiation from a dipole embedded in a multilayer slab is studied theoretically, and in Ref. 26 optical measurements are made on a system consisting of either silver or indium nanoparticles embedded in a thin amorphous silicon film on top of a quartz substrate. In the present work, plasmon resonances of nanospheres near a surface or embedded in a thin layer are studied. Under the assumption that the radius of the nanosphere is very small compared to the wavelength, we present an efficient scheme for calculating particle plasmon eigenfrequencies and absorption cross sections. Our scheme is based on the Green's function surface integral approach, which compared to, e.g., FDTD or FE has an advantage in scattering problems because, by choosing an appropriate Green's function, only the surface of the nanosphere has to be discretized.

The paper is organized as follows. In Sec. II the theoretical approach for calculating particle plasmon eigenfrequencies and absorption cross sections is presented. Sec. III presents the results, where silver spheres both above a silicon surface and within silicon film is analyzed. Both eigenvalues and absorption cross section spectra are calculated. In Sec. IV we offer our conclusions.

II. GREEN'S FUNCTION SURFACE INTEGRAL EQUATION APPROACH

Several Green's function surface integral equation approaches for studying electromagnetic and quantum-mechanical problems involving nanoparticles, nanostructures, and nanocavities are known see, e.g., Refs. 23 and 27–37. Usually the Green's function surface integral equation method relates the field at any position inside a closed domain to the field and its normal derivative on the surface of the domain by means of surface integral equations, and individual domains are related via the boundary conditions. For light scattering from, e.g., a metallic nanoparticle Ω placed in an open infinite domain Γ (see Fig. 1) the method

 ©2010 The American Physical Society

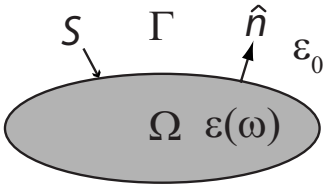

FIG. 1. Schematic of the elements involved in the surface integral equation method. The Ω region represents a nanoparticle with a surface S, an outward normal $\hat{n}$, and a frequency dependent relative dielectric constant $\varepsilon(\omega)$. The surrounding medium is Γ and is described by the relative dielectric constant ε_0.

is an appropriate and efficient choice because, as mentioned in the introduction, the analysis simply reduces to an integral over the surface S of Ω. In an electrostatic analysis the surface integral equations can with advantage be formulated in terms of the electrostatic potential $\phi(\mathbf{r})$ because this yields a set of scalar equations. We wish to demonstrate that the apparently different formalisms; the nonretarded version of the approach introduced in, e.g., Ref. 22 and the approach of Ref. 37 do, in fact, lead to identical surface integral equations. Following this, the surface integral equations are solved for a number of important cases.

We start our discussion by introducing the electrostatic potential which is related to the electrostatic electric field as $\mathbf{E}(\mathbf{r})=-\nabla\phi(\mathbf{r})$. The electrostatic potential must in each domain fulfill Laplace's equation

$$\nabla^2\phi(\mathbf{r})=0 \quad \forall \quad \mathbf{r}, \tag{1}$$

with the boundary conditions (cf. Fig. 1)

$$\phi_\Omega=\phi_\Gamma, \quad \varepsilon(\omega)\frac{\partial\phi_\Omega}{\partial n}=\varepsilon_0\frac{\partial\phi_\Gamma}{\partial n} \quad \text{on} \quad S, \tag{2}$$

where $\partial/\partial n=\hat{n}\cdot\nabla$. If we define a Green's function $g(\mathbf{r},\mathbf{r}')$ satisfying

$$\nabla^2 g(\mathbf{r},\mathbf{r}')=-\delta(\mathbf{r}-\mathbf{r}'), \tag{3}$$

where $\delta(\mathbf{r})$ is the Dirac delta function, it is straightforward, using Green's second integral identity, to show that a set of surface integral equations in terms of the electrostatic potential can be formulated as[23,28,31,35]

$$\phi(\mathbf{r})=\phi_0(\mathbf{r})+\oint_S\left[\phi(\mathbf{s}')\frac{\partial g(\mathbf{r},\mathbf{s}')}{\partial n'}-g(\mathbf{r},\mathbf{s}')\frac{\partial\phi_\Gamma(\mathbf{s}')}{\partial n'}\right]dS' \quad \text{for} \quad \mathbf{r}\in\Gamma,$$

$$\phi(\mathbf{r})=-\oint_S\left[\phi(\mathbf{s}')\frac{\partial g(\mathbf{r},\mathbf{s}')}{\partial n'}-g(\mathbf{r},\mathbf{s}')\frac{\varepsilon_0}{\varepsilon(\omega)}\frac{\partial\phi_\Gamma(\mathbf{s}')}{\partial n'}\right]dS' \quad \text{for} \quad \mathbf{r}\in\Omega, \tag{4}$$

where $\partial/\partial n'=\hat{n}'\cdot\nabla'$, $\hat{n}$ is the outward normal of Ω, $\phi_0(\mathbf{r})$ is the incident potential, and $\mathbf{s}$ is a point belonging to the surface S of Ω. By means of Eq. (4) the potential at positions outside and inside Ω can be calculated. However, before Eq. (4) can be used, the field and its normal derivative on the surface of Ω must be known. These can be calculated from the self-consistent equations obtained by letting the point $\mathbf{r}$ in Eq. (4) approach the surface S from either sides $\mathbf{r}\to\mathbf{s}$. This yields

$$\frac{1}{2}\phi(\mathbf{s})=\phi_0(\mathbf{s})+\mathrm{PV}\oint_S\phi(\mathbf{s}')\frac{\partial g(\mathbf{s},\mathbf{s}')}{\partial n'}dS'-\oint_S g(\mathbf{s},\mathbf{s}')\frac{\partial\phi_\Gamma(\mathbf{s}')}{\partial n'}dS',$$

$$\frac{1}{2}\phi(\mathbf{s})=-\mathrm{PV}\oint_S\phi(\mathbf{s}')\frac{\partial g(\mathbf{s},\mathbf{s}')}{\partial n'}dS'+\oint_S g(\mathbf{s},\mathbf{s}')\frac{\varepsilon_0}{\varepsilon(\omega)}\frac{\partial\phi_\Gamma(\mathbf{s}')}{\partial n'}dS', \tag{5}$$

where PV refers to Cauchy's principal value. The singularity at $\mathbf{s}=\mathbf{s}'$ of $\partial g(\mathbf{s},\mathbf{s}')/\partial n'$ is handled by rewriting the part of the integrals involving this term as principal value integrals. At the singularity these integrals yield $\pm\phi(\mathbf{s})/2$ for a smooth surface element where the $\pm$ depends on from which domain $\mathbf{r}$ approaches the surface S. Note that the formulation of the surface integral equations in Eq. (5) is very similar to the formulation of the scalar surface integral equations of the magnetic field for p polarization as formulated in. e.g., Refs. 23 and 35. The formulation in these two references includes retardation effects but is only suitable for two-dimensional problems, whereas the formulation in terms of the potential in Eq. (5) can be used to analyze three-dimensional structures in the electrostatic limit. The self-consistent surface integral equations of Eq. (5) can be further simplified if we rewrite in terms of the surface polarization charge density $\sigma(\mathbf{s})=\epsilon_0\left(\frac{\partial\phi_\Omega(\mathbf{s})}{\partial n}-\frac{\partial\phi_\Gamma(\mathbf{s})}{\partial n}\right)$, where ϵ_0 is the vacuum permittivity. If we take the normal derivative of both equations and add them together using the boundary conditions of Eq. (2) we obtain

$$\sigma(\mathbf{s})-\lambda\oint_S h(\mathbf{s},\mathbf{s}')\sigma(\mathbf{s}')dS'=2\epsilon_0\lambda\hat{n}\cdot\mathbf{E}_0, \tag{6}$$

where $\mathbf{E}_0$ is the amplitude vector of the incident electric field and the parameter λ is given as

$$\lambda=\frac{\varepsilon(\omega)-\varepsilon_0}{\varepsilon(\omega)+\varepsilon_0}. \tag{7}$$

In order to obtain Eq. (6) we have also introduced an integral kernel as

$$h(\mathbf{s},\mathbf{s}')=-2\frac{\partial g(\mathbf{s},\mathbf{s}')}{\partial n}. \tag{8}$$

If there is no incident field Eq. (6) reduces to the following homogenous surface integral eigenvalue equation

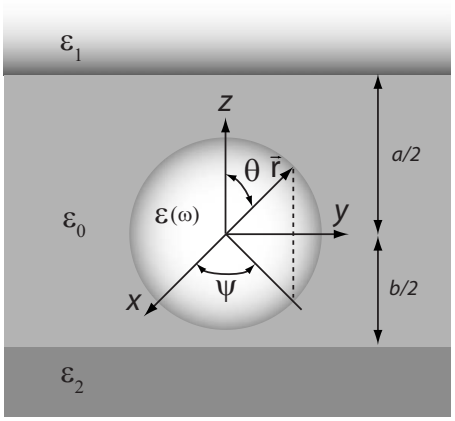

FIG. 2. A metallic nanosphere situated inside a thin film.

$$\sigma(\mathbf{s}) - \lambda \oint_S h(\mathbf{s},\mathbf{s}')\sigma(\mathbf{s}')dS' = 0. \tag{9}$$

Both Eqs. (6) and (9) have been presented before, see e.g., Refs. 37–40. However, it has not been pointed out that the approach of Eq. (6) is identical to the standard approach of Eq. (5).

The nontrivial solutions $\sigma_i(\mathbf{s})$ of Eq. (9) specifies the eigenvalues $1/\lambda_i$, which through the knowledge of $\varepsilon(\omega)$ allows for calculation of the eigenfrequencies of the surface plasmon eigenmodes supported by Ω. If we assume that the dielectric constant of Ω is of the canonical Drude form $\varepsilon(\omega) = \varepsilon_\infty - \omega_p^2/\omega^2$, the relation between the eigenvalue and the resonance frequency is given as

$$\omega_i = \frac{\omega_p}{\sqrt{\varepsilon_\infty + \varepsilon_0 \dfrac{\lambda_i + 1}{\lambda_i - 1}}}. \tag{10}$$

It is important to notice that because we are in the electrostatic limit, where the Green's function is independent of the materials optical properties [see Eq. (3)], this is also the case for the entire surface integral in Eqs. (6) and (9).

In the following we use Eqs. (6) and (9) to extend the work of Ref. 37 and others, in order to analyze layered geometries, where the particle is situated within a thin film. For spherical particles we present an efficient scheme that allows for calculation of both plasmon eigenfrequencies and absorption cross sections by means of a single integral along the polar angle of the sphere. The specific configuration that we analyze is a metallic nanosphere described by a frequency dependent relative dielectric constant $\varepsilon(\omega)$ situated inside a thin film of thickness $(a+b)/2$ with optical properties described by the relative dielectric constant ε_0. The relative dielectric constants of the two media above and below the film are ε_1 and ε_2, respectively, and the origin of the coordinate system is chosen to coincide with the center of the nanosphere. The distance from the center of the nanosphere to the lower boundary of the film is $b/2$ and to the top boundary it is $a/2$. In all calculations we assume that $a/2 > R$ and $b/2 > R$, where R is the radius of the nanosphere (Fig. 2).

With the method of electrostatic images in mind it is straightforward to show that the Green's function that we must use in Eqs. (6) and (9) in order to incorporate the two boundaries of the reference medium is, cf. Fig. 2, given as

$$\begin{aligned} h(\mathbf{s},\mathbf{s}') &= \frac{-\hat{n}\cdot\nabla}{2\pi}\left[\frac{1}{|\mathbf{s}-\mathbf{s}'|} + \frac{\beta_1}{|\mathbf{s}-\mathbf{s}'_M - a\hat{z}|} + \frac{\beta_2}{|\mathbf{s}-\mathbf{s}'_M + b\hat{z}|} + \frac{\beta_1\beta_2}{|\mathbf{s}-\mathbf{s}'+(a+b)\hat{z}|} + \ldots\right] \\ &= \frac{\hat{n}\cdot}{2\pi}\left[\frac{\mathbf{s}-\mathbf{s}'}{|\mathbf{s}-\mathbf{s}'|^3} + \beta_1\frac{\mathbf{s}-\mathbf{s}'_M - a\hat{z}}{|\mathbf{s}-\mathbf{s}'_M - a\hat{z}|^3} + \beta_2\frac{\mathbf{s}-\mathbf{s}'_M + b\hat{z}}{|\mathbf{s}-\mathbf{s}'_M + b\hat{z}|^3} + \beta_1\beta_2\frac{\mathbf{s}-\mathbf{s}'+(a+b)\hat{z}}{|\mathbf{s}-\mathbf{s}'+(a+b)\hat{z}|^3} + \ldots\right], \end{aligned} \tag{11}$$

where β_i are given as

$$\beta_i = \frac{\varepsilon_0 - \varepsilon_i}{\varepsilon_0 + \varepsilon_i}, \tag{12}$$

and $\mathbf{s}$ and $\mathbf{s}'$ are points belonging to the surface S of the sphere, and $\mathbf{s}'_M$ is the mirrored version of $\mathbf{s}'$ about $z=0$. As a consequence of the symmetry of the problem the surface polarization charge density can be expanded as $\sigma(\mathbf{r}) = \sigma(r,\theta)\exp(im\psi)$, where m is an integer. This is because $\sigma(\mathbf{r})$ must be 2π periodic in ψ in order to ensure the azimuthal periodicity of the structure. We only look for dipolar solutions with $m=0$ and $m=\pm 1$ as higher-order modes are very difficult to excite. If we measure all distances in units of the sphere radius, this implies for $m=0$ to search for solutions that only depend on θ, and for $m=\pm 1$ solutions that vary as $\cos\psi$ times a function of θ. $m=0$ modes with a vertically polarized particle dipole moment can be excited if the incident electric field is directed along $\hat{z}$, and $m=\pm 1$ modes with a horizontally polarized particle dipole moment can be excited if the incident electric field e.g., is directed along $\hat{x}$. In order to comply with this we may choose [cf. Fig. 2]

$$\hat{n}(\theta) = \mathbf{s}(\theta) = \sin\theta\hat{x} + \cos\theta\hat{z},$$

$$\mathbf{s}'(\theta',\psi') = \sin\theta'\cos\psi'\hat{x} + \sin\theta'\sin\psi'\hat{y} + \cos\theta'\hat{z},$$

$$\mathbf{s}'_M(\theta',\psi') = \mathbf{s}'(\pi-\theta',\psi'). \tag{13}$$

By contemplating the integral kernel of Eq. (11) we see that in order to eliminate the ψ dependence, we need to evaluate reduced kernel terms of the form

$$H_a^{(v)}(\theta,\theta') = \int_0^{2\pi} \frac{\hat{n}\cdot(\mathbf{s}-\mathbf{s}'-a\hat{z})}{2\pi|\mathbf{s}-\mathbf{s}'-a\hat{z}|^3}d\psi',$$

$$H_a^{(h)}(\theta,\theta') = \int_0^{2\pi} \frac{\hat{n}\cdot(\mathbf{s}-\mathbf{s}'-a\hat{z})\cos\ \psi'}{2\pi|\mathbf{s}-\mathbf{s}'-a\hat{z}|^3}d\psi', \tag{14}$$

where (v) and (h) are applied for vertically and horizontally polarized particle dipole moments, respectively. By substituting the vectors from Eq. (13) into Eq. (14) it is easy to show that the results can be expressed in terms of the elementary integrals

$$F_{m,n}(x,y) \equiv \int_0^{2\pi} \frac{\cos^m\ \psi'}{(x+y\ \cos\ \psi')^{(2n+1)/2}}d\psi', \tag{15}$$

with $x=1+a^2/2+a(\cos\ \theta'-\cos\ \theta)-\cos\ \theta\cos\ \theta'$ and $y=-\sin\ \theta\sin\ \theta'$. Such integrals can be expressed by means of the complete elliptic integrals of first and second kind, $K(\alpha)$ and $E(\alpha)$, respectively, if the argument is $\alpha=2y/(x+y)$, see Appendix. Thus the reduced kernel terms for the two polarizations can be expressed as

$$H_a^{(v)}(\theta,\theta') = \frac{1}{4\pi\sqrt{2}}\left[F_{0,0}(x,y) - \left(\frac{1}{2}a^2 + a\ \cos\ \theta'\right)F_{0,1}(x,y)\right],$$

$$H_a^{(h)}(\theta,\theta') = \frac{1}{4\pi\sqrt{2}}\left[F_{1,0}(x,y) - \left(\frac{1}{2}a^2 + a\ \cos\ \theta'\right)F_{1,1}(x,y)\right], \tag{16}$$

which for $a=0$ are given as

$$H_0^{(v)}(\theta,\theta') = \frac{K\left(\dfrac{2\ \sin\ \theta\ \sin\ \theta'}{\cos(\theta-\theta')-1}\right)}{\pi\sqrt{2[1-\cos(\theta-\theta')]}},$$

$$H_0^{(h)}(\theta,\theta') = \frac{1}{\pi\sqrt{2[1-\cos(\theta-\theta')]}} \times\left[\frac{\cos(\theta-\theta')-1}{\sin\ \theta\ \sin\ \theta'}E\left(\frac{2\ \sin\ \theta\ \sin\ \theta'}{\cos(\theta-\theta')-1}\right) - \frac{\cos\ \theta\cos\ \theta'-1}{\sin\ \theta\ \sin\ \theta}K\left(\frac{2\ \sin\ \theta\ \sin\ \theta'}{\cos(\theta-\theta')-1}\right)\right]. \tag{17}$$

Using Eqs. (11), (16), and (17) the full reduced kernel can be expressed as

$$H(\theta,\theta') = H_0(\theta,\theta') + \beta_1 H_a(\theta,\pi-\theta') + \beta_2 H_{-b}(\theta,\pi-\theta') + \beta_1\beta_2 H_{-(b+a)}(\theta,\theta') + \ldots \tag{18}$$

Thus, the surface integral equation of Eq. (6) can be rewritten in a reduced form, where the azimuthal dependence is analytically integrated. The reduced form of the surface integral equation is given as

$$\sigma(\theta) - \lambda\int_0^{\pi} H(\theta,\theta')\sigma(\theta')\sin\ \theta'd\theta' = 2\epsilon_0\lambda\hat{n}\cdot\mathbf{E}_0, \tag{19}$$

where $\hat{n}\cdot\mathbf{E}_0$ is $E_0\cos\ \theta$ for vertical polarization and $E_0\sin\ \theta$ for horizontal polarization. In the case of eigenvalue analysis, the right-hand side with the source term is zero. To some extent, a similar approach has recently been used to reduce the number of dimensions in Ref. 41, where a surface integral approach was used to calculate absorption spectra from small cylindrical gold rods. However, only for $m=0$.

From Eq. (17) it can be seen that the $H_0(\theta,\theta')$ term of the integral kernel is singular for $\theta=\theta'$. In order to deal with this singularity we split the full kernel $H(\theta,\theta')$ in a direct, singular part $H_0(\theta,\theta')$ and an indirect, nonsingular part $I(\theta,\theta')$ such that $H(\theta,\theta')=H_0(\theta,\theta')+I(\theta,\theta')$. If we define

$$S_0(\theta) \equiv \int_0^{\pi} H_0(\theta,\theta')\sin\ \theta'd\theta', \tag{20}$$

which for vertically and horizontally polarized particle dipole moments is given as

$$S_0^{(v)}(\theta) = 1,$$

$$S_0^{(h)}(\theta) = -\frac{1}{8}\sum_{m=0}^{\infty}\left(\frac{\Gamma\left(m+\dfrac{1}{2}\right)}{(m+1)!}\right)^2 P_{2m+1}^1(\cos\ \theta), \tag{21}$$

respectively, where $P_m^n(x)$ is the associated Legendre polynomial and $\Gamma(x)$ is the complete gamma function, we can rewrite the reduced surface integral equation in a nonsingular form as

$$\sigma(\theta) - \lambda\left[S_0(\theta)\sigma(\theta) + \int_0^{\pi} H_0(\theta,\theta')[\sigma(\theta')-\sigma(\theta)]\sin\ \theta'd\theta' + \int_0^{\pi} I(\theta,\theta')\sigma(\theta')\sin\ \theta'd\theta'\right] = 2\epsilon_0\lambda\hat{n}\cdot\mathbf{E}_0, \tag{22}$$

where again $\hat{n}\cdot\mathbf{E}_0$ is $E_0\cos\ \theta$ and $E_0\sin\ \theta$ for vertical and horizontal polarization, respectively.

The optical absorption is calculated by means of the particle dipole moment $\mathbf{p}$, which can be calculated from knowledge of the electric field inside the particle as

$$\mathbf{p} = \epsilon_0(\varepsilon(\omega)-\varepsilon_0)\int_V \mathbf{E}(\mathbf{r})dV = \varepsilon_0\oint_S \mathbf{s}\sigma(\mathbf{s})dS, \tag{23}$$

where the boundary conditions and the divergence theorem have been used to rewrite the volume integral of the electric field over the particle to a surface integral involving the surface polarization charge density. With Eq. (13) and the above symmetry considerations in mind, we can express the particle dipole moment for vertical and horizontal polarization as

$$p^{(v)} = 2\pi\varepsilon_0\int_0^{\pi}\sigma(\theta)\cos\ \theta\sin\ \theta d\theta,$$

$$p^{(h)} = \pi\varepsilon_0 \int_0^{\pi} \sigma(\theta)\sin^2\theta d\theta, \tag{24}$$

respectively. Finally, we can calculate the absorption cross section as the time-averaged power lost due to absorption in the particle (Ohmic losses) normalized with the magnitude of the Poynting vector of the incident field. For plane wave incidence this yields

$$\sigma_{abs}(\omega) = \frac{\omega\ \mathrm{Im}[\mathbf{p}\cdot\mathbf{E}_0^*]}{c\epsilon_0\sqrt{\varepsilon_0}|E_0|^2}, \tag{25}$$

where c is the speed of light in vacuum. Equation (25) is, in fact, an expression for the extinction cross section (the sum of the scattering cross section and the absorption cross section) for a small particle with the approximation

$$\epsilon_0[\varepsilon(\omega)-\varepsilon_0]\int_V \mathbf{E}(\mathbf{r})\cdot\mathbf{E}_0^*(\mathbf{r})dV \approx \mathbf{p}\cdot\mathbf{E}_0^*. \tag{26}$$

For a purely real dielectric constant our electrostatic approach neglects a small phase difference between $\mathbf{p}$ and $\mathbf{E}_0$ and thus Eq. (25) is only apt to account for the absorption in the particle.

For numerical purposes we discretize using the following Gauss-Laguerre quadrature $\theta\rightarrow\theta_i$, $\theta\rightarrow\theta_j$, and $\int(\ldots)d\theta' \rightarrow\Sigma_j(\ldots)w_j$.[42] Thus

$$\frac{1}{\lambda}\sigma(\theta_i) - S_0(\theta_i)\sigma(\theta_i) - \sum_{j\neq i} H_0(\theta_i,\theta_j)[\sigma(\theta_j)-\sigma(\theta_i)]\sin\theta_j w_j - \sum_j I(\theta_i,\theta_j)\sigma(\theta_j)\sin\theta_j w_j = 2\epsilon_0\hat{n}_i\cdot\mathbf{E}_0, \tag{27}$$

where $\hat{n}_i\cdot\mathbf{E}_0$ is $E_0\cos\theta_i$ for vertical polarization and $E_0\sin\theta_i$ for horizontal polarization. In the case of eigenvalue analysis this implies that we look for eigensolutions of a matrix with elements

$$H_{ij} = I(\theta_i,\theta_j)\sin\theta_j w_j + \begin{cases} S_0(\theta_i) - \sum_{k\neq i} H_0(\theta_i,\theta_k)\sin\theta_k w_k & \text{for } i=j \\ H_0(\theta_i,\theta_j)\sin\theta_j w_j & \text{for } i\neq j \end{cases}, \tag{28}$$

whereas if we are interested in the optical absorption it implies that we solve a matrix equation on the form $\mathbf{Ax}=\mathbf{b}$, where $\mathbf{A}$ is given as

$$\mathbf{A} = \frac{1}{\lambda}\mathbf{I} - \mathbf{H}, \tag{29}$$

where $\mathbf{H}$ has elements as specified in Eq. (28), $\mathbf{I}$ is the identity matrix, the elements of $\mathbf{b}$ are $b_i=2\epsilon_0 E_0\cos\theta_i$ for vertical polarization and $b_i=2\epsilon_0 E_0\sin\theta_i$ for horizontal polarization, and the elements of the solution vector $\mathbf{x}$ are $x_i=\sigma(\theta_i)$.

III. RESULTS

Using the surface integral approach outlined in Sec. II, we analyze silver nanospheres in two different configurations.

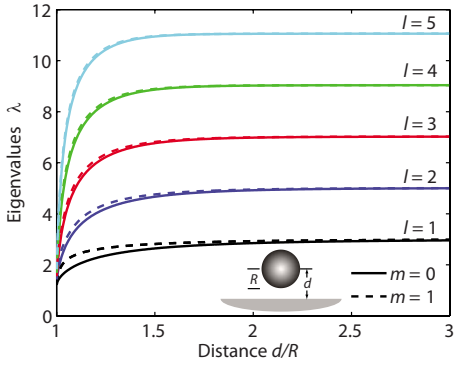

FIG. 3. (Color online) The first five ($l=1$ to 5) resonant eigenvalues of a metallic sphere of radius R above a silicon surface. d is the distance between the center of the sphere and the surface, see inset, and the dielectric constants of the reference medium are $\varepsilon_0=\varepsilon_1=1$ and $\varepsilon_2=12$. See Fig. 2.

Above a silicon surface and within a silicon film which is situated on top of a quartz substrate. The latter configuration coincides with the structure studied experimentally in Ref. 26. In all calculations, we used a simple Drude formula

$$\varepsilon(\omega) = \varepsilon_\infty - \frac{\omega_p^2}{\omega(\omega+i\Gamma)}, \tag{30}$$

with $\varepsilon_\infty=5.0$, $\hbar\omega_p=9.3$ eV, and $\hbar\Gamma=0.1$ eV, in order to model the spectral dependence of the dielectric constant of the silver nanospheres. The silicon and quartz media are modeled as dispersionless lossless dielectrics with dielectric constants of 12 and 2.25, respectively. As scattering and eigenvalue analysis of three-dimensional plasmonic nanostructures usually is a time (CPU) consuming task, it is important to point out that the electrostatic approach presented above is quite efficient. For example, a full converged absorption cross section spectrum for 500 wavelengths can be calculated in a few seconds using Intel Math Kernel Library (MKL) routines and standard Fortran 95. In all calculations 200 quadrature points are used along θ and 20 terms of the infinite sum are included in the calculation of $S_0^{(h)}(\theta)$, see Eq. (21). For spheres within a thin film the first nine terms are included in the Green's function of Eq. (11).

A. Sphere above a silicon surface

We have calculated the first five eigenvalues (numbered $l=1$ to 5)[43] of a metallic nanosphere placed a distance $d-R$ from a silicon surface (Fig. 3), where R is the radius of the sphere and d is the distance between the center of the sphere and the silicon surface (see inset of Fig. 3). Such a configuration can easily be analyzed with the scheme outlined in Sec. II. The difference from the film configuration is that only two terms must be included in the Green's function [Eq. (11)], a direct propagation and an indirect propagation which accounts for the interaction with the surface. The eigenvalues are calculated both for vertically ($m=0$) and horizontally ($m=1$) polarized surface plasmon resonances. Again we stress that the eigenvalues are decoupled from the optical properties of the metallic nanosphere. The influence of $\varepsilon(\omega)$

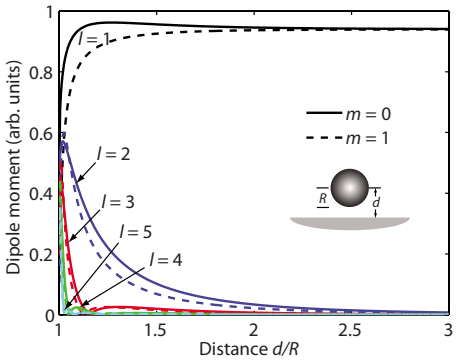

FIG. 4. (Color online) The dipole moment associated with the first five ($l=1$ to 5) eigenmodes versus the sphere-surface separation. The dipole moments are normalized by means of Eq. (31). For details of the configuration see the caption of Fig. 3.

does not enter before the eigenvalues are converted into plasmon resonance frequencies by means of Eq. (10). For large sphere-surface separations ($d/R>3$) the eigenvalues of the two polarizations are practically degenerate, as in the case of an isolated sphere, meaning that the particle plasmon resonances of the sphere are almost decoupled from the surface. However, when decreasing the separation the degeneracy between the two polarizations is lifted and the eigenvalues start to decrease. With Eq. (10) in mind a decreasing eigenvalue corresponds to a redshift of the plasmon resonance frequency. By contemplating the results it can be seen that vertically polarized surface plasmon resonances are redshifted more than horizontally polarized resonances. Note also that the eigenvalues of nanosphere plasmons with a large l are bending more than the eigenvalues of nanosphere plasmons with a small l when the sphere approaches the surface. We have compared our calculation of the eigenvalues for the sphere-surface configuration with the result of an analysis of a metal nanosphere in the vicinity of a metal surface with an infinite plasmon frequency which was presented in Ref. 17. An excellent agreement was found.

Given the eigenvectors belonging to the eigenvalues it is possible, by means of Eq. (24), to calculate the dipole moments associated with the individual eigenmodes. Normalizing such that

$$\oint_S |\sigma(\theta)\cos(m\psi)|dS = 1, \tag{31}$$

where $dS=\sin\theta d\theta d\psi(R^2)$, the first five dipole moments have been calculated as a function of the sphere-surface separation for $m=0$ and 1 (Fig. 4). Because the presence of the surface breaks the spherical symmetry, eigenmodes with $l>1$, which for a sphere in a homogenous surrounding are symmetry forbidden, are allowed. This is clearly seen in Fig. 4. For large sphere-surface separations ($d/R>3$) all the dipole moments for eigenmodes with $l>1$ are vanishing and the two $l=1$ dipole moments are degenerate. For intermediate distances ($1.1<d/R<2$) the dipole moment of the $l=2$ mode increases significantly, and as the sphere gets very close to the surface ($|d/R-1|\ll 1$) even the $l=3$, 4, and 5 dipole modes become important.

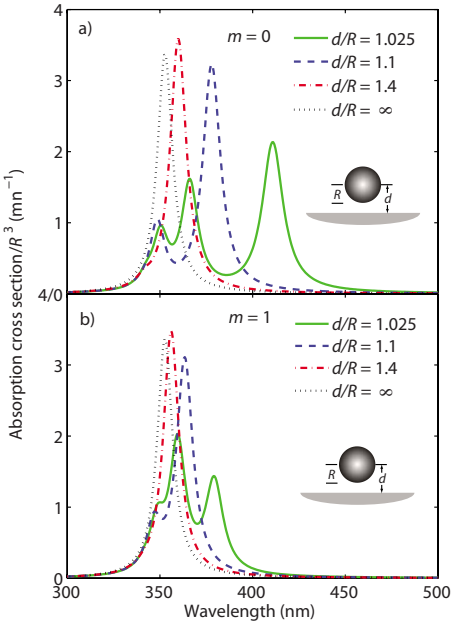

FIG. 5. (Color online) The absorption cross section spectrum for different distances to the silicon surface. (a) $m=0$. (b) $m=1$. For details of the configuration see the caption of Fig. 3

In order to study the optical absorption of the sphere-surface configuration we have calculated the absorption cross section $\sigma_{abs}(\omega)$ using Eq. (25). First for vertically polarized induced dipole moments $m=0$, where the incident electric field is directed along the z axis [Fig. 5(a)]. Four different separations d/R are depicted, three where the sphere is relatively close to the surface (the separation is below the radius of the nanosphere) and one where the separation is infinite. As expected from the eigenvalue analysis, the optical absorption peak redshifts as the silver sphere approaches the silicon surface. The presence of resonances with $l>1$ is clearly seen in the absorption cross-section spectrum when the sphere is close to the surface. For $d/R=1.1$ (dashed/blue curve) two peaks are seen in the spectrum, one large around 380 nm and a smaller at 350 nm. By comparing Fig. 5(a) to Figs. 3 and 4 it can be concluded that the two peaks corresponds to the $l=1$ and 2 eigenmodes. For $d/R=1.025$ (solid/green curve) at least three distinct resonance peaks appear, and it is seen how the oscillator strength of the $l=1$ resonance around 410 nm is reduced because it is distributed over several resonances with $l>1$. For horizontally polarized induced dipole moments, where $m=1$ and the incident electric field is directed perpendicular to the z axis, the absorption cross section spectrum is depicted for four separations in Fig. 5(b). All the same tendencies as for vertically induced dipole moments are seen in the spectra. The resonances redshift and more resonance peaks emerge as the sphere approaches the surface. When comparing with vertical polarization [Fig. 5(a)], we see, as expected from the eigenvalue analysis, that the redshift is smaller. As a result a smaller splitting between the resonances with different l is observed. For $d/R=1.025$ it can be noted that the $l=2$ resonance is stronger than the $l=1$.

In order to fully illustrate the dependence of the optical absorption on the sphere-surface separation we have made a contour plot of the spectrum versus the separation for d/R

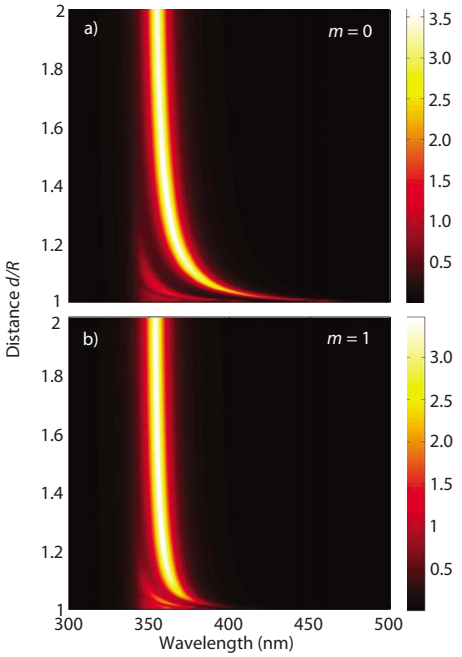

FIG. 6. (Color online) The absorption cross section spectrum versus the distance from the center of the sphere to the silicon surface. For details of the configuration see the caption of Fig. 3.

ranging from 1 to 2 for both $m=0$ and $m=1$ (Fig. 6). The contour plot illustrates how the $l=1$ resonance continuously redshifts as the sphere approaches the surface. For short separations it can also be seen how resonances with $l>1$ emerge and grow as the separation is reduced. Again it is clear that the redshift of the resonances is considerably smaller for horizontal polarization.

B. Silver sphere within a silicon film

We analyze a sphere-in-slab configuration where a silver nanosphere is embedded within a thin silicon film which is placed on top of a quartz substrate. The thickness of the silicon film is $2d$ and the sphere of radius R is placed in the

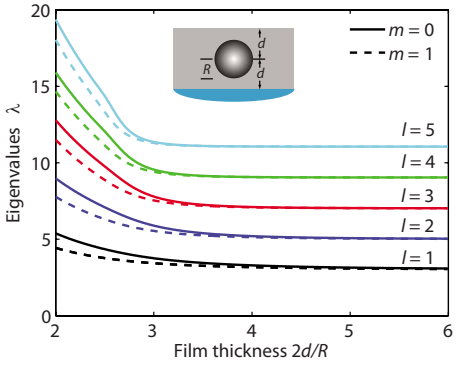

FIG. 7. (Color online) The first five ($l=1$ to 5) resonant eigenvalues of a metallic sphere of radius R situated at the center of a silicon film of thickness $2d$. The silicon film is placed on top of a quartz substrate. The dielectric constants of the silicon film, the air above, and the quartz substrate are $\varepsilon_0=12$, $\varepsilon_1=1$, and $\varepsilon_2=2.25$, respectively.

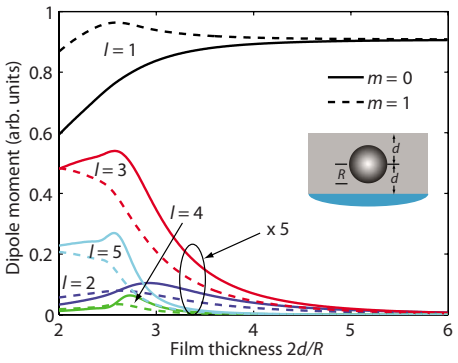

FIG. 8. (Color online) The dipole moment associated with the lowest five ($l=1$ to 5) eigenmodes versus the film thickness. The dipole moments are normalized by means of Eq. (31). In the figure the curves for $l=2$ to 5 have been scaled with a factor of 5 for better visualization. For details of the configuration see the caption of Fig. 7

center of the film. The lowest five eigenvalues for both polarizations versus the film thickness is depicted in Fig. 7. For $2d/R>6$ the configuration closely resembles an isolated sphere, where the eigenvalues of the two polarizations are degenerate and take the values 3, 5, 7, 9, and 11 when l is varied from 1 to 5. As the film thickness is decreased the two polarizations split up and the eigenvalues increase, which corresponds to a blueshift of the sphere plasmon resonances. As for the sphere-surface configuration the largest shift is seen for vertically polarized eigenmodes. We have also calculated the individual dipole moments of the eigenmodes for the sphere-in-slab configuration (Fig. 8). Again as the two surfaces of the film and the asymmetry introduced by the difference in ε_1 and ε_2 have broken the spherical symmetry, resonances with $l>1$ are symmetrically allowed in the sphere-in-slab configuration. This effect is clearly seen in the calculation of the dipole moments of the individual eigenmodes, where eigenmodes with $l>1$ gain a dipole moment as the film thickness is reduced. However, the $l=1$ eigenmode has by far the largest dipole moment for all film thicknesses. All higher degree dipolar modes have a dipole moment that is at least a factor of 5 smaller than the dipole moment of the $l=1$ mode, even for small film thicknesses close to the diameter of the nanosphere. Note that resonances with an odd l have significantly larger dipole moments than resonances with an even l. The dipole moments of the even eigenmodes ($l=2$ and 4) are actually decreasing for film thicknesses below approximately 2.5 in units of the sphere radius.

For the sphere-in-slab configuration the calculated absorption cross sections are related to the incident field E_0, which is the electric field within the slab. For vertical polarized-induced dipole moments the absorption cross section spectrum is presented for four different film thicknesses in Fig. 9(a). As expected from the dipole moments of the individual eigenmodes (Fig. 8), all four spectra are dominated by the $l=1$ resonance. As the film thickness is reduced the resonance blueshifts. For films with thicknesses close to the diameter of the sphere the dipolar resonances of $l>1$ modes become visible in the spectrum as small shoulders to the left

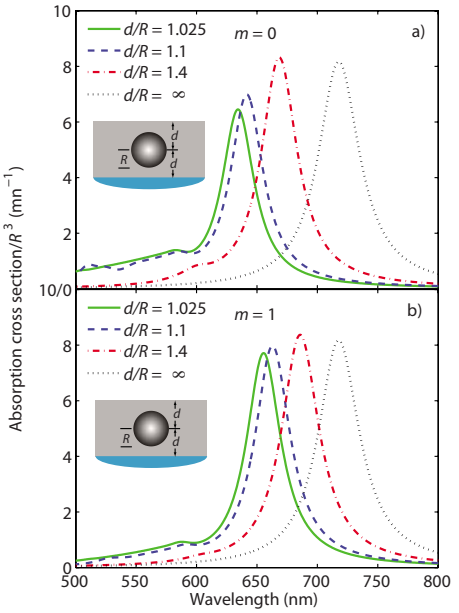

FIG. 9. (Color online) The absorption cross section spectrum for different film thicknesses. (a) m is 0. (b) $m=1$. For details of the configuration see the caption of Fig. 7.

of the large $l=1$ resonance. A contour plot of the absorption cross section spectrum versus the film thickness is presented in Fig. 10(a) for $m=0$. It can be seen that the resonance continuously blueshifts as the film thickness is reduced. A total blueshift of approximately 90 nm from ~720 to ~630 nm is observed when the silicon film thickness is reduced to 2 in units of the sphere radius. Note that two effects

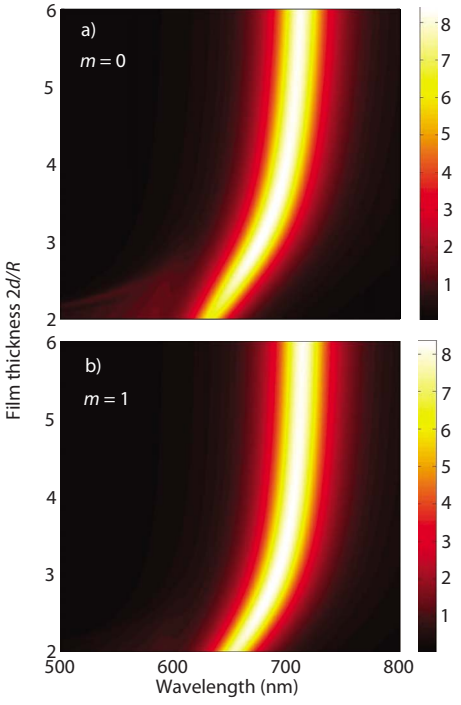

FIG. 10. (Color online) The absorption cross-section spectrum versus the thickness of the silicon film. (a) m is 0. (b) m is 1. For details of the configuration see the caption of Fig. 7.

are involved in the resonance shift when the film thickness is reduced. From the results presented in Fig. 5, we know that when the sphere approaches an interface the nanosphere plasmon resonances redshift. However, when the thickness of the silicon film is reduced the sphere is not only getting closer to the interfaces, the effective refractive index of the surrounding is also reduced. Hence, the free space wavelength must be smaller (blueshifted) if the resonance wavelength must be the same. The calculations show that the combination of the two mechanisms results in a blueshift when the thickness of the film is reduced.

For horizontally polarized induced dipole moments the absorption cross section spectrum versus the film thickness is presented in Fig. 9(b) for four different thicknesses and as a contour plot in Fig. 10(b). As expected from the eigenvalue analysis the blueshift as the film thickness is reduced is smaller for horizontal polarization than for vertical polarization. A total blueshift of 70 nm from ~720 to ~650 nm is observed. This calculation can be directly compared to the experiment presented in Ref. 26, where the resonances of silver nanoclusters incorporated into a thin sputtered amorphous silicon film on top of a quartz plate are measured. For comparison, the measured resonance shifts from approximately 740 nm for thick films to around 550 nm for film thicknesses in the order of the size of the silver nanoclusters. A possible explanation of the slightly larger resonance wavelength for thick films can be that the dielectric constant of amorphous silicon is slightly larger than the dielectric constant of 12 used in our calculations. If, e.g., the dielectric constant of the amorphous silicon is 15 the $l=1$ plasmon resonance redshifts to ~790 nm. An explanation of the larger blueshift observed in the experiment can be that the silver particles are sticking out of the amorphous silicon film when the film thickness is comparable to the diameter of the particles in the experiment. If this is the case, the plasmon resonance frequencies will most likely change.

In solar cell applications particle plasmon resonances in the near infrared part of the spectrum are desirable.[7] For the sphere-in-slab configuration a resonance at 720 nm is achieved when the film is thick. Importantly, our results (cf. Figs. 7–10) show how thin the film can be made before the resonance starts to move toward lower wavelengths. This is an important design aspect for plasmon enhanced solar cells.

IV. CONCLUSION

In conclusion, we have presented an efficient method for analysis of electrostatic plasmon resonances of a metallic nanosphere situated in a layered geometry. The method is a surface integral approach for the surface polarization charge density that allows for calculation of both the source free plasmonic eigenmodes and, in the presence of an external field, the absorption cross-section spectrum. By means of symmetry considerations the three-dimensional problem is reduced to a single integral along the polar angle of the sphere, as all effects of the stratified surrounding are built into the Green's function. The approach is exemplified by studying the eigenmodes and the optical absorption of silver nanospheres, first above a silicon surface and second within a

thin silicon film on top of a quartz substrate. In the first configuration a redshift of the fundamental $l=1$ resonance is observed as the sphere approaches the surface. In the latter configuration the resonance blueshifts as the film thickness is reduced. As the presence of the surface(s) breaks the spherical symmetry of the problem, plasmon resonances with $l>1$ that usually are symmetry forbidden become allowed. This effect is, e.g., clearly seen in the sphere-surface configuration, where several resonances emerge in the absorption cross section spectrum when the sphere is close to the surface. For horizontally polarized induced dipole moments the $l=2$ resonance even dominates the $l=1$ resonance for small sphere-surface separations. Note that a method as presented in this work, which can be used for exact analysis of the electrostatic optical absorption of nanoparticles buried within thin films, is an important development step toward the realization of efficient plasmon enhanced solar cells.

ACKNOWLEDGMENTS

The authors gratefully acknowledge the financial support from the project "Localized-surface plasmons and silicon thin-film solar cells—PLATOS" which is financed by the Villum Foundation.

APPENDIX: REDUCED KERNEL TERMS

The individual terms of the reduced kernel can be expressed in terms of the elementary integrals

$$F_{m,n}(x,y) \equiv \int_0^{2\pi} \frac{\cos^m \psi'}{(x+y\cos\psi')^{(2n+1)/2}} d\psi'. \tag{A1}$$

The first few of these are given as

$$F_{0,0}(x,y) = \frac{4}{\sqrt{x+y}} K\left(\frac{2y}{x+y}\right), \tag{A2}$$

$$F_{0,1}(x,y) = \frac{4}{(x-y)\sqrt{x+y}} E\left(\frac{2y}{x+y}\right), \tag{A3}$$

$$F_{1,0}(x,y) = \frac{4\sqrt{x+y}}{y} E\left(\frac{2y}{x+y}\right) - \frac{4x}{y\sqrt{x+y}} K\left(\frac{2y}{x+y}\right), \tag{A4}$$

where $K(x)$ and $E(x)$ are the complete elliptic integrals of first and second kind defined as

$$K(x) \equiv \int_0^{\pi/2} [1 - x\sin^2\theta]^{-1/2} d\theta, \tag{A5}$$

$$E(x) \equiv \int_0^{\pi/2} [1 - x\sin^2\theta]^{1/2} d\theta, \tag{A6}$$

respectively. Higher terms of $F_{m,n}(x,y)$ can be generated using

$$F_{m,n}(x,y) = \frac{F_{m-1,n-1}(x,y) - xF_{m-1,n}(x,y)}{y}. \tag{A7}$$

*jung@nano.aau.dk

[1] D. M. Schaadt, B. Feng, and E. T. Yu, Appl. Phys. Lett. **86**, 063106 (2005).
[2] S. Pillai, K. R. Catchpole, T. Turpke, and M. A. Green, J. Appl. Phys. **101**, 093105 (2007).
[3] D. Derkacs, S. H. Lim, P. Mathue, W. Mar, and E. T. Yu, Appl. Phys. Lett. **89**, 093103 (2006).
[4] C. Hägglund, M. Zäch, and B. Kasemo, Appl. Phys. Lett. **92**, 013113 (2008).
[5] J. S. Biteen, N. S. Lewis, and H. A. Atwater, Appl. Phys. Lett. **88**, 131109 (2006).
[6] K. R. Catchpole and A. Polman, Opt. Express **16**, 21793 (2008).
[7] K. R. Catchpole and A. Polman, Appl. Phys. Lett. **93**, 191113 (2008).
[8] S. Lal, S. Link, and N. J. Halas, Nature Photon. **1**, 641 (2007).
[9] M. Moskovits, Rev. Mod. Phys. **57**, 783 (1985).
[10] Y. C. Cao, R. Jin, and C. A. Mirkin, Science **297**, 1536 (2002).
[11] A. J. Haes and R. P. V. Duyne, J. Am. Chem. Soc. **124**, 10596 (2002).
[12] L. Lorenz, K. Dan. Vidensk. Selsk., Mat-Fys. Skr. **6**, 1 (1890).
[13] G. Mie, Ann. Phys. **330**, 377 (1908).
[14] M. M. Wind, J. Vlieger, and D. Bedeaux, Physica A **141**, 33 (1987).
[15] G. Videen, M. G. Turner, V. J. Iafelice, W. S. Bickel, and W. L. Wolfe, J. Opt. Soc. Am. A **10**, 118 (1993).
[16] V. V. Gozhenko, L. G. Grechko, and K. W. Whites, Phys. Rev. B **68**, 125422 (2003).
[17] P. Nordlander and E. Prodan, Nano Lett. **4**, 2209 (2004).
[18] I. A. Larkin, M. I. Stockman, M. Achermann, and V. I. Klimov, Phys. Rev. B **69**, 121403(R) (2004).
[19] A. Pinchuk and G. Schatz, Nanotechnology **16**, 2209 (2005).
[20] Y. Pavlyukh and W. Hübner, Appl. Phys. A: Mater. Sci. Process. **82**, 67 (2006).
[21] A. Taflove and S. Hagness, *Computational Electrodynamics: The Finite-Difference Time-Domain Method* (Artech House, Boston, 2000).
[22] J. Jin, *The Finite Element Method in Electromagnetics*, 2nd ed. (Wiley, New York, 2002).
[23] T. Søndergaard, Phys. Status Solidi B **244**, 3448 (2007).
[24] O. J. F. Martin, C. Girard, and A. Dereux, Phys. Rev. Lett. **74**, 526 (1995).
[25] S. R. J. Brueck, V. A. Smagley, and P. G. Eliseev, Phys. Rev. E **68**, 036608 (2003).
[26] O. Stenzel, A. Stendal, M. Röder, and C. V. Borczyskowski, Pure Appl. Opt. **6**, 577 (1997).
[27] P. A. Knipp and T. L. Reinecke, Phys. Rev. B **54**, 1880 (1996).
[28] D. W. Prather, M. S. Mirotznik, and J. N. Mait, J. Opt. Soc. Am. A Opt. Image Sci. Vis. **14**, 34 (1997).
[29] D. W. Prather, J. N. Mait, M. S. Mirotznik, and J. P. Collins, J. Opt. Soc. Am. A Opt. Image Sci. Vis. **15**, 1599 (1998).

[30] I. V. Novikov and A. A. Maradudin, Phys. Rev. B **66**, 035403 (2002).
[31] J. Wiersig, J. Opt. A, Pure Appl. Opt. **5**, 53 (2003).
[32] P. I. Geshev, S. Klein, T. Witting, K. Dickmann, and M. Hietschold, Phys. Rev. B **70**, 075402 (2004).
[33] P. I. Geshev and K. Dickmann, J. Opt. A, Pure Appl. Opt. **8**, S161 (2006).
[34] U. Hohenester and J. Krenn, Phys. Rev. B **72**, 195429 (2005).
[35] J. Jung and T. Søndergaard, Phys. Rev. B **77**, 245310 (2008).
[36] A. M. Kern and O. J. F. Martin, J. Opt. Soc. Am. A Opt. Image Sci. Vis. **26**, 732 (2009).
[37] I. D. Mayergoyz, D. R. Fredkin, and Z. Zhang, Phys. Rev. B **72**, 155412 (2005).
[38] I. D. Mayergoyz and Z. Zhang, IEEE Trans. Magn. **42**, 759 (2006).
[39] Z. Zhang, I. D. Mayergoyz, N. A. Gumerov, and R. Duraiswami, IEEE Trans. Magn. **43**, 1465 (2007).
[40] I. D. Mayergoyz, Z. Zhang, and G. Miano, Phys. Rev. Lett. **98**, 147401 (2007).
[41] C. Pecharromán, J. Pérez-Juste, G. Mata-Osoro, L. M. Liz-Marzán, and P. Mulvaney, Phys. Rev. B **77**, 035418 (2008).
[42] W. H. Press, S. A. Teukolsky, W. T. Vetterling, and B. P. Flannery, *Numerical Recipes: The Art of Scientific Computing*, 3rd ed. (Cambridge University Press, New York, 2007).
[43] Note that for a sphere in a homogenous surrounding l is the degree of the spherical harmonic eigenfunction and a well-behaved number. Strictly speaking, this is not true in the sphere-surface configuration. However, the eigenvectors and eigenvalues can still be numbered according to the size of the eigenvalue.